Spectral Patterns of Chaotic Acetylene†

John P. Rose and Michael E. Kellman*

Department of Chemistry, University of Oregon, Eugene, Oregon 97403

Received: April 14, 2000; In Final Form: June 26, 2000

A diabatic correlation diagram procedure, first applied (Rose, J. P.; Kellman, M. E., *J. Chem. Phys.* **1996**, *105*, 7348) to H_2O, is used to classify energy and intensity patterns in the highly excited bending spectrum of C_2H_2, modeled by an effective spectroscopic fitting Hamiltonian. Analysis with polyad phase spheres accounts for the observed patterns in terms of classical phase space structure and bifurcations of the low-energy normal modes.

Introduction

This paper is about detecting and understanding new kinds of patterns in spectra in which very high vibrations are excited, in particular, in the molecule C_2H_2. With sufficient excitation, the low-energy normal modes analysis becomes severely inadequate, due to the interplay of anharmonicity and multiple resonance couplings. Dramatic changes take place in the dynamics, including the abrupt birth of new anharmonic modes in bifurcations from the original normal modes, and the onset of widespread chaotic classical dynamics. This results in severe disturbance of the spectral patterns associated with normal modes.

Here, we explore novel patterns in high-energy spectra as represented by an effective spectral fitting Hamiltonian, developed by a number of workers to analyze experiments on the C_2H_2 molecule. We use a version of the Hamiltonian employed by Field and co-workers.[1,2]

Several groups,[3−5,8−10] following early indications[11,12] on the basis of theoretical analysis of the C_2H_2 spectroscopic Hamiltonian, have succeeded in unraveling the spectrum into distinct sets of levels characterized by the "polyad", or total vibrational quantum number. Here, we seek to identify and understand patterns *within* the polyads. There is no a priori justification to search for patterns at the subpolyad level, since there are no rigorous quantum numbers known that would be related to such patterns, even at the level of approximation inherent in the structure of the spectroscopic Hamiltonian. Nonetheless, we have easily succeeded in identifying approximate subpolyad patterns in H_2O, using a correlation diagram technique.[13]

Nearly simultaneously with the present paper, we have devised a "dressed basis" approach[14] to highly excited vibrations, and tested it with success on H_2O. The dressed basis approach puts the empirical correlation diagram procedure on a much sounder conceptual footing. Here, we proceed again in a frankly empirical vein with correlation diagram techniques for C_2H_2, but now making appeal to dressed basis ideas.

We find that there are novel energy and intensity patterns within subpolyads of the polyads with 10, 12, and 14 quanta of bending vibration. We are able to account for these patterns with a Hamiltonian that describes energy flow along the "primary" energy transfer pathway induced by an effective Darling−Dennison coupling. This success in a portion of the spectrum strongly motivates a quest for a comprehensive analysis for the entire spectrum, even up to the barrier to isomerization to vinylidene, using a technique such as the dressed basis.

II. Are There Novel Patterns in Highly Excited Spectra?

To be as concrete as possible, we examine some suggestive features of the C_2H_2 spectrum predicted in a simulation of the dispersed fluorescence spectrum using the spectroscopic Hamiltonian. This is an effective Hamiltonia used to fit experimental data. This Hamiltonian has been developed over several decades by a variety of workers. Since the 1990s, it has been progressively refined to fit large quantities of high-energy data obtained in absorption, dispersed fluorescence, and SEP experiments. (Absorption probes regions of phase space complementary to those accessed by fluorescence and SEP experiments.) We use a version of the Hamiltonian employed by Field and co-workers[1,2] at a particular stage of refinement of the empirical fitting parameters. The Hamiltonian is described in full detail in section IV.

After the calculations reported in this paper, these parameters have been modified somewhat by various workers[4,6−10] in response to new experimental data, and in all likelihood will be refined further. We are confident that all the basic conclusions here will stand as the Hamiltonian is further refined in response to new data.

Figure 1 shows a stick-spectrum simulation, using the spectroscopic Hamiltonian, of part of the experimental dispersed fluorescence spectrum. In these experiments, a Franck−Condon transition from an upper electronic state follows excitation from the electronic ground state. This results in excitation of a vibrational wave packet on the ground state, i.e., a superposition of excited "bright" zero-order vibrational states, with zero quanta in all modes except the C−C stretch ν_2 and the trans-bend ν_4. Figure 1 shows the portion of the spectrum with $n_2 = 0$ and $n_4 = 8-16$, with the vibrational angular momentum $l = 0$. It should be compared with the corresponding $n_2 = 0$ part of Figure 2 of ref 3 of Solina et al. (Comparisons of direct absorption and dispersed fluorescence spectra of very similar polyads were reported contemporaneously by Herman and co-workers.[9]) Their

† Part of the special issue "C. Bradley Moore Festschrift".

* Corresponding author. E-mail: kellman@oregon.uoregon.edu.

10.1021/jp001424i CCC: $19.00
Published on Web 08/30/2000

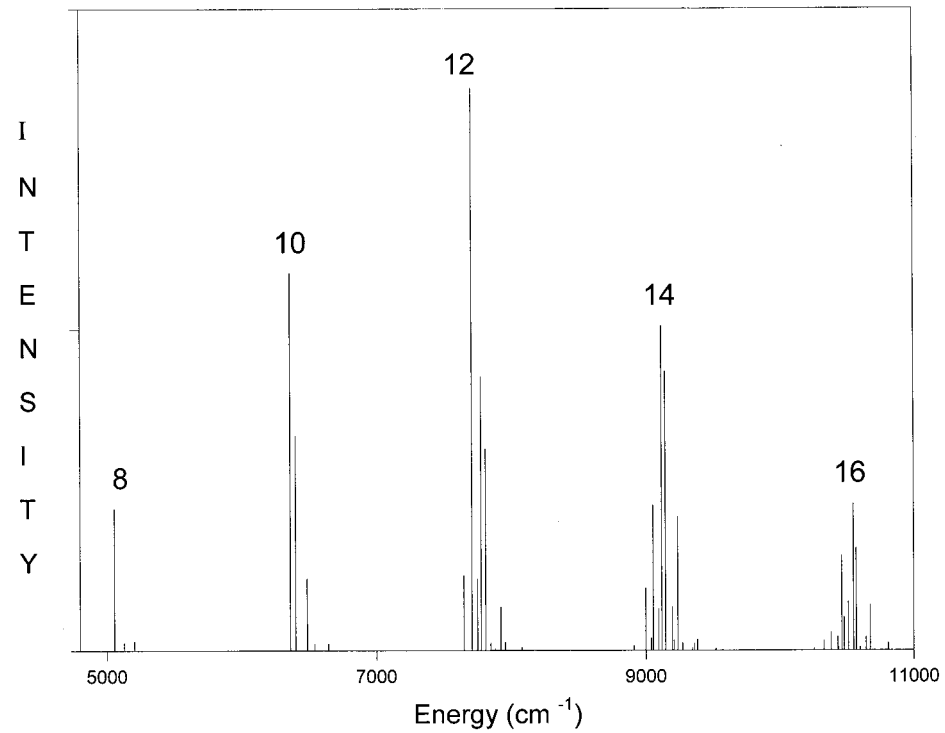

Figure 1. Simulation of dispersed fluorescence spectrum of C_2H_2 with $\nu_2 = 0$ and $\nu_4 = 6-18$. The clusters of levels are polyads originating from a zero-order bright state for each ν_4.

figure exemplifies an analysis in which experimental spectra were "unzipped" into polyads of levels, each polyad originating from a different zero-order bright state. (That each polyad originates from a *single* zero-order bright state is a simplification which certainly does not necessarily hold in general, but which has proven empirically[3−5] to be valid for the C_2H_2 dispersed fluorescence spectra considered here.) Each of the five clumps of levels in Figure 1 is a distinct polyad with $n_2 = 0$, and labeled by the number of ν_4 quanta (= 8−16) in the zero-order bright state from which the polyad originates. The spectrum of Figure 1 is complicated, with intensity in many features, because the resonance couplings in the spectroscopic Hamiltonian break the ν_4 quantum number, and "fractionate" the intensity of each bright zero-order state (0, 0, 0, n_4, 0).

Close inspection of Figure 1 hints at patterns *within* the individual polyads. As an example, Figure 2 shows a detail of polyad 14 from Figure 1. It appears as if there might be a sequence of levels of especially high intensity, as well as one or more sequences of less intense levels. These patterns are not as clear-cut as in low-energy spectra, where sequences are typically "cleaner" in appearance, and clearly identifiable by means of normal modes quantum number assignments. In Figure 2, several possible sequences are plausibly identifiable. However, this identification is by no means clear-cut, and there are several reasonable possibilities. Another revealing view of the spectrum comes with a logarithmic plot. This is shown in Figure 16b, which will be the focus of detailed discussion and interpretation in section X. One of our goals is a more systematic method in place of this "eyeball" pattern identification.

We make use of an earlier[15] bifurcation analysis of highly excited acetylene bends coupled by a single Darling−Dennison resonance. This work showed that the bending dynamics exhibits a new type of correlated motion called "precessional" modes, in addition to the more familiar normal and local modes.

Although the work in ref 15 used a simplified, single-resonance model, it is decisive here for understanding the

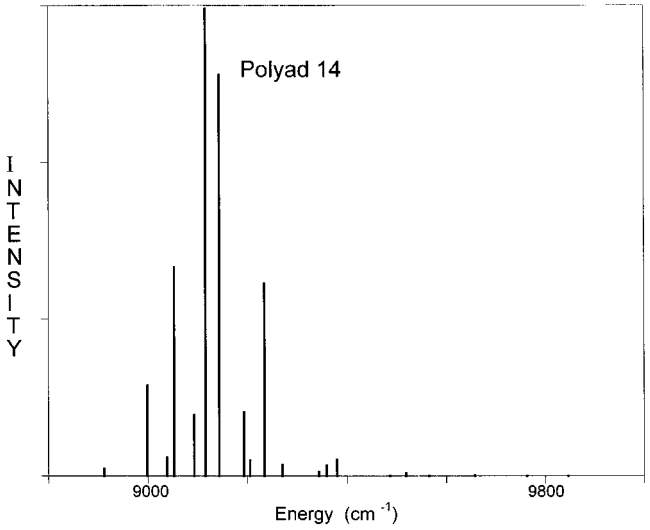

Figure 2. Detail from Figure 1 of polyad with $\nu_4 = 14$. The same spectrum is shown on a logarithmic scale in Figure 16b.

observed energy and intensity patterns of the experimental spectrum, within a framework that now takes account of the other degrees of freedom and resonant couplings. This requires the diabatic correlation diagram technique, which is outlined next.

III. Assigning Spectra Beyond Polyads

The correlation diagram technique developed out of an approach to highly excited spectra using bifurcation analysis of the spectroscopic Hamiltonian. In bifurcations, the low-energy normal modes become unstable and branch into new anharmonic modes, due to the interplay of the anharmonicity of the normal modes and their mutual couplings.

Knowledge of the internal molecular dynamics decoded from the spectrum via the bifurcation analysis is used to construct "dynamical" assignments of quantum numbers for the newly identified modes. These assignments are then used to identify spectral patterns.[16] This approach was first applied[15−26] to a number of systems with a single-resonance coupling and nonchaotic dynamics.

A key extension was analysis of three modes coupled by multiple resonances with classical chaos, as in H_2O. One of the salient findings[27] was that for many systems, including H_2O, the bifurcation structure can be decomposed into a sequence of independent two-mode bifurcations, similar, despite the nonintegrability and chaos of the system, to those observed for systems with a single resonance between two modes.

This simplification led to an empirical assignment procedure using diabatic correlation diagrams.[13] The result is assignment of a complete, though approximate and nonrigorous, set of "nominal" or "effective" quantum numbers. These quantum numbers can be used to group the levels in various ways into sets of subpolyads, or sequences.

To better understand the physical meaning of this subpolyad classification with nominal assignments, we have investigated a "dressed basis" approach.[14] The zero-order basis is dressed by all the resonance couplings in the effective Hamiltonian, except for a residual coupling $\hat{\mathbf{V}}_i$. Acting within subpolyads of the dressed basis, an effective coupling $\hat{\mathbf{V}}_i^{\text{eff}}$ is defined in correspondence to the residual $\hat{\mathbf{V}}_i$.

The goal of the dressed basis is to incorporate as much as possible the effects of nonintegrability, while retaining much of the simplicity of integrable systems via the effective residual single-resonance coupling. This is useful to the extent that the eigenstates of the spectroscopic Hamiltonian are approximated by those of the new effective Hamiltonian. Numerical testing[14] shows that the procedure works remarkably well.

In the next two sections we describe the spectroscopic Hamiltonian and how it leads to natural organizations of the zero-order spectrum into subpolyads, as a prelude to applying the diabatic correlation diagram assignment to classify and interpret spectral patterns of the eigenstate spectrum of the full Hamiltonian.

IV. Spectroscopic Hamiltonian

This section describes the spectroscopic Hamiltonian for acetylene, taking advantage of an important simplification, the separation of stretch and bend modes, which is justified[6,15] for the spectra we want to analyze, where all the excitation is placed initially in the bend modes.

Acetylene has seven vibrational modes: symmetric C−H stretch ν_1, C−C stretch ν_2, antisymmetric C−H stretch ν_3, doubly degenerate C−H trans-bend ν_4, and doubly degenerate C−H cis-bend ν_5. The degenerate bend modes can be represented in either a rectilinear zero-order basis with modes ν_{ja} and ν_{jb} or in an angular momentum basis with modes ν_{j+} and ν_{j-} ($j = 4, 5$). In this paper we will use the angular momentum basis. In this basis the states are designated by the quantum numbers $n_j = n_{j+} + n_{j-}$ and $l_j = n_{j+} - n_{j-}$. With these quantum numbers, the zero-order states are labeled by the quantum numbers (n_1, n_2, n_3, n_4, l_4; n_5, l_5).

The full spectroscopic Hamiltonian for the highly excited, $J = 0$ vibrational energy levels of acetylene consists of a diagonal part, $\hat{\mathbf{H}}_0$, and an off-diagonal part, $\hat{\mathbf{V}}$:

$$\hat{\mathbf{H}} = \hat{\mathbf{H}}_0 + \hat{\mathbf{V}} \tag{1}$$

TABLE 1: Bend−bend Resonance Couplings for Acetylene

1. Darling−Dennison bend resonance I	$\hat{\mathbf{V}}_{\text{DD-I}} = K_{\text{DD-I}}[\mathbf{a}_{4+}^{\dagger}\mathbf{a}_{4-}^{\dagger}\mathbf{a}_{5+}\mathbf{a}_{5-} + \text{h.c.}]$ $\Delta n_4 = -\Delta n_5 = 2,\ \Delta l_4 = \Delta l_5 = 0$
2. Darling−Dennison bend resonance II	$\hat{\mathbf{V}}_{\text{DD-II}} = \hat{\mathbf{V}}_{\text{DD-IIa}} + \hat{\mathbf{V}}_{\text{DD-IIb}}$ $\hat{\mathbf{V}}_{\text{DD-IIa}} = {}^1/_4 K_{\text{DD-II}}[\mathbf{a}_{4+}^{\dagger}\mathbf{a}_{4+}^{\dagger}\mathbf{a}_{5+}\mathbf{a}_{5+} + \text{h.c.}]$ $\Delta n_4 = -\Delta n_5 = 2,\ \Delta l_4 = -\Delta l_5 = 2$ $\hat{\mathbf{V}}_{\text{DD-IIb}} = {}^1/_4 K_{\text{DD-II}}[\mathbf{a}_{4-}^{\dagger}\mathbf{a}_{4-}^{\dagger}\mathbf{a}_{5-}\mathbf{a}_{5-} + \text{h.c.}]$ $\Delta n_4 = -\Delta n_5 = 2,\ \Delta l_4 = -\Delta l_5 = -2$
3. vibrational-l resonance	$\hat{\mathbf{V}}_{\text{vib}-l} = K_{\text{vib}-l}[\mathbf{a}_{4+}^{\dagger}\mathbf{a}_{4-}\mathbf{a}_{5+}\mathbf{a}_{5-}^{\dagger} + \text{h.c.}]$ $\Delta n_4 = \Delta n_5 = 0,\ \Delta l_4 = -\Delta l_5 = 2$

The diagonal part represents the harmonic and anharmonic contributions to the vibrational energy levels

$$\hat{\mathbf{H}}_0 = \sum_{j=1}^{5}\omega_j(n_j + d_j) + \sum_{j=1}^{5}\sum_{k=j}^{5}\chi_{jk}(n_j + d_j)(n_k + d_k) + \sum_{j=4}^{5}\sum_{k=j}^{5}g_{jk}l_jl_k \tag{2}$$

where ω_j is the harmonic frequency for mode j, n_j is the number of vibrational quanta in mode j, d_j is the zero-point energy contribution for mode j ($d_j = {}^1/_2$ for $j = 1-3$ and $d_j = 1$ for $j = 4, 5$), and χ_{jk} is the anharmonicity constant between modes j and k.

The off-diagonal part $\hat{\mathbf{V}}$ contains the spectroscopically significant collection of mode−mode resonance couplings, i.e., those needed to fit the data to the desired or attainable level of detail and accuracy. Parameters for the coupling strengths are determined in the fitting of the spectrum. Many resonances have been detected in acetylene spectra using various excitation techniques.[28−30]

It is found empirically that the pure bend zero-order bright states whose spectra we are analyzing are coupled only to zero-order states that involve the four bend modes. This means that for bright states that are pure bending, the system can be viewed as decoupled from the stretches, and analyzed independently, as noted previously.[6,15] We can therefore work with just the pure bend portion $\hat{\mathbf{H}}_{\text{bend}}$ of the full Hamiltonian:

$$\hat{\mathbf{H}}_{\text{bend}} = \hat{\mathbf{H}}_0 + \hat{\mathbf{V}}_{\text{DD-I}} + \hat{\mathbf{V}}_{\text{DD-IIa}} + \hat{\mathbf{V}}_{\text{DD-IIb}} + \hat{\mathbf{V}}_{\text{vib}-l} \tag{3}$$

The bend−bend resonance couplings of $\hat{\mathbf{H}}_{\text{bend}}$ are listed in detail in Table 1. The $\hat{\mathbf{V}}_{\text{DD-I}}$, $\hat{\mathbf{V}}_{\text{DD-IIa}}$, and $\hat{\mathbf{V}}_{\text{DD-IIb}}$ resonances are referred to as 2:2 Darling−Dennison resonances because they exchange two quanta of action between the trans- and cis-bend modes. We will refer to the symmetry pair $\hat{\mathbf{V}}_{\text{DD-IIa}}$ and $\hat{\mathbf{V}}_{\text{DD-IIb}}$ together as $\hat{\mathbf{V}}_{\text{DD-II}}$. Independently these two resonances are not symmetry allowed, but together they have the correct symmetry. The coupling $\hat{\mathbf{V}}_{\text{vib}-l}$ does not look quite like a 2:2 Darling-Dennison resonance, but rather like a product of 1:1 resonances, that is, a 1:1 resonance between the two degenerate trans-bend modes ($\Delta n_{4+} = \Delta n_{4-} = \pm 1$) and simultaneously a 1:1 resonance between the two degenerate cis-bend modes ($\Delta n_{5+} = -\Delta n_{5-} = \pm 1$).

The values for the spectroscopic parameters, including diagonal terms of eq 2 as well as the strengths of the resonance couplings in Table 1, are given in Table 2. These parameters are those reported by Jonas et al.,[1] and subsequently modified very slightly by Jonas.[2]

V. Subpolyads and Coupling Pathways

This section describes "slicings" of the polyads of $\hat{\mathbf{H}}_0$ into subpolyads, arising naturally from the coupling pathways of the

TABLE 2: Molecular Constants (cm^{-1})

$\omega_1 = 3509.895$	$\chi_{12} = -12.62$	$\chi_{24} = -12.48$	$\chi_{11} = -2.406$
$\omega_2 = 2012.51$	$\chi_{13} = -105.09$	$\chi_{25} = -1.57$	$\chi_{11} = -2.335$
$\omega_3 = 3414.745$	$\chi_{14} = -15.58$	$\chi_{33} = -27.41$	$g_{44} = 0.759$
$\omega_4 = 622.768$	$\chi_{15} = -10.85$	$\chi_{34} = -6.96$	$g_{45} = 6.541$
$\omega_5 = 746.801$	$\chi_{22} = -7.39$	$\chi_{35} = -8.69$	$g_{55} = 3.49$
$\chi_{11} = -25.87$	$\chi_{23} = -6.10$	$\chi_{44} = 3.082$	
$K_{DD-I} = -10.0$	$K_{DD-I} = 6.844$	$K_{vib-l} = -6.238$	

empirical spectroscopic Hamiltonian, that will be useful later in uncovering and analyzing spectral patterns. The focus in this section is on polyads and subpolyads of the zero-order Hamiltonian $\hat{\mathbf{H}}_0$; this subpolyad organization will form a template for classifying the eigenstates of $\hat{\mathbf{H}}_{bend}$ in section VI and beyond.

The polyad numbers are constants of motion of the spectroscopic Hamiltonian that remain after taking into account the resonance couplings, which break the individual normal modes quantum numbers. The polyads describe small sets of states in which the spectroscopic Hamiltonian is diagonal. The method for finding the polyad numbers has been described earlier[11,31] and used extensively for acetylene.[3−5,8−12]

The polyad numbers are special combinations of the zero-order quantum numbers. For example, for C_2H_2 in a simplified five-mode notation that neglects the vibrational angular momentum, the total polyad number

$$N = 5n_1 + 3n_2 + 5n_3 + n_4 + n_5 \tag{4}$$

is a constant of the spectroscopic Hamiltonian.

For our system, there are five quantities that are conserved by $\hat{\mathbf{H}}_{bend}$: n_1, n_2, n_3, and

$$P = n_{4+} + n_{4-} + n_{5+} + n_{5-} = n_4 + n_5 \tag{5}$$

$$l = n_{4+} - n_{4-} + n_{5+} - n_{5-} = l_4 + l_5 \tag{6}$$

P is the total number of quanta in the bend modes, and l the total vibrational angular momentum. These are very convenient for spectra of the bends-only Hamiltonian $\mathbf{H}_{bend}$. A "total" quantum number such as (4) or its seven-mode generalization[8,9] for the Hamiltonian $\hat{\mathbf{H}}$ of (3) can easily be constructed from combinations of the quantum numbers $\{n_1, n_2, n_3, P, l\}$.

For the polyads treated in this paper, $n_1 = n_2 = n_3 = l = 0$. Consequently, we can specify the different polyads by the single, total bend quantum number P. Within polyads, zero-order states are specified by the quantum numbers (n_4, l_4; n_5, l_5).

It is convenient to define slicings of the polyad into subpolyads by the action of the resonance couplings of the spectroscopic Hamiltonian. Each of the resonances $\hat{\mathbf{V}}_{DD-I}$, $\hat{\mathbf{V}}_{DD-II}$, $\hat{\mathbf{V}}_{vib-l}$ of $\hat{\mathbf{H}}_{bend}$ in (3) couples states within a particular kind of subpolyad slicing (or "net", in the case of $\hat{\mathbf{V}}_{DD-II}$.) These coupling pathways are shown for polyad 10 in Figure 3. The Darling−Dennison−I resonance $\hat{\mathbf{V}}_{DD-I}$ is shown as the vertical bold coupling, indicating the "primary" energy transfer pathway from the bright zero-order state. $\hat{\mathbf{V}}_{DD-I}$ is primary because the other couplings are weaker in their effect on the energy spectrum, or else do not connect directly to the bright zero-order state. In Figure 3, $\hat{\mathbf{V}}_{DD-I}$ couples levels in the "stack" (n_4, l_4; n_5, l_5) = (10,0;0,0), (8,0;2,0) . . . (0,0;10,0).

Next, we use diabatic correlation diagrams to classify the *eigenstates* of the spectrum of $\mathbf{H}_{bend}$ into subpolyads analogous to the slicings of the zero-order Hamiltonian by $\hat{\mathbf{V}}_{DD-I}$ and $\hat{\mathbf{V}}_{vib-l}$. A very preliminary account along these lines for C_2H_2 has appeared previously.[32]

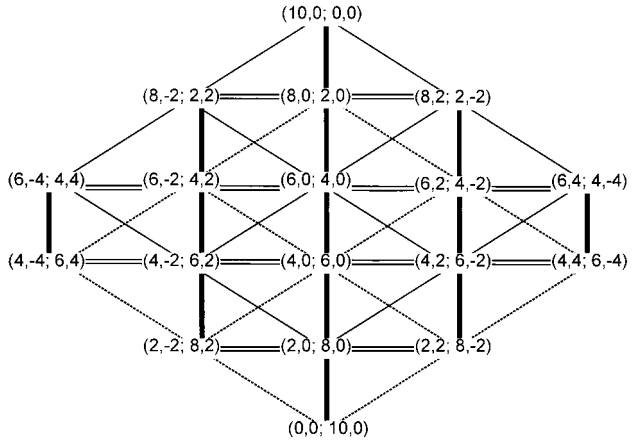

Figure 3. Resonance coupling pathways in polyad 10. $\hat{\mathbf{V}}_{DD-I}$, shown as vertical bold coupling, is the primary energy transfer pathway from the bright zero-order state (10, 0; 0, 0). $\hat{\mathbf{V}}_{vib-l}$ is horizontal coupling pathway; $\hat{\mathbf{V}}_{DD-IIa,b}$ is diagonal coupling pathway.

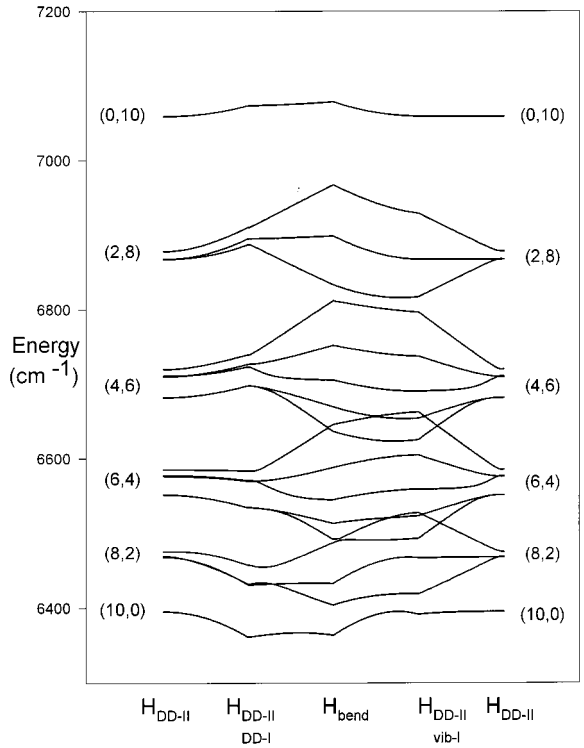

Figure 4. Adiabatic correlation diagram for polyad 10 showing levels of various partial Hamiltonians, with levels of full bend Hamiltonian in center.

VI. Diabatic Correlation Diagram Assignments

Figure 4 starts with *adiabatic* curves for a relatively simple case, polyad 10. The original zero-order states of $\hat{\mathbf{H}}_0$ are completely labeled by the bend quantum numbers (n_4, l_4; n_5, l_5). The bright state of the polyad is the zero-order state (10, 0; 0, 0). For economy, Figure 4 does not actually show the zero-order energies, but merely indicates the zero-order states with common (n_4, n_5) at the left and right; the zero-order levels happen to cluster into these sets. For example, (8, 2) represents the three zero-order levels (8, −2; 2, 2), (8, 0; 2, 0), and (8, 2; 2, −2). We then turn on the resonance couplings in various sequences. One sequence is shown at the left in Figure 4 starting with the least important resonance coupling $\hat{\mathbf{V}}_{DD-II}$ turned on first, i.e., its strength is started at zero and increased to 100% of its value in the spectroscopic Hamiltonian $\mathbf{H}_{bend}$. We next turn on $\hat{\mathbf{V}}_{DD-I}$, the Darling-Dennison coupling between the

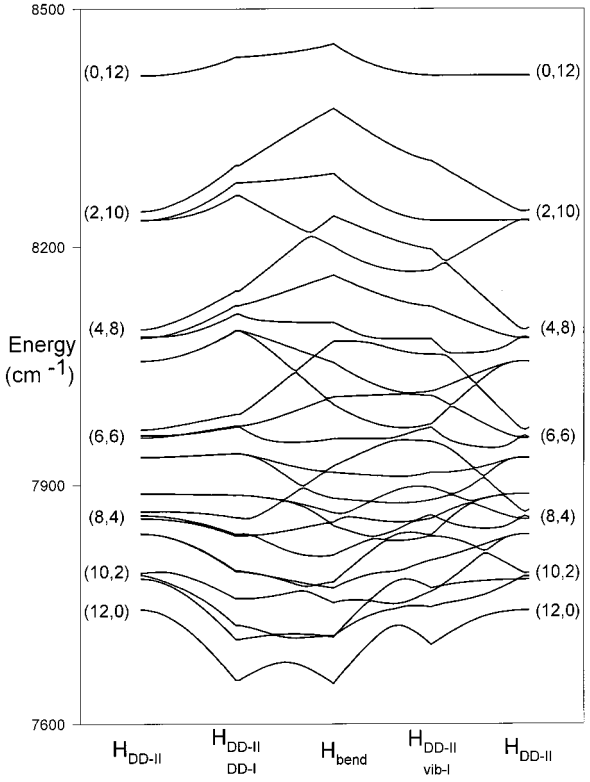

Figure 5. Adiabatic correlation diagram for polyad 12 showing levels of various partial Hamiltonians, with levels of full bend Hamiltonian in center.

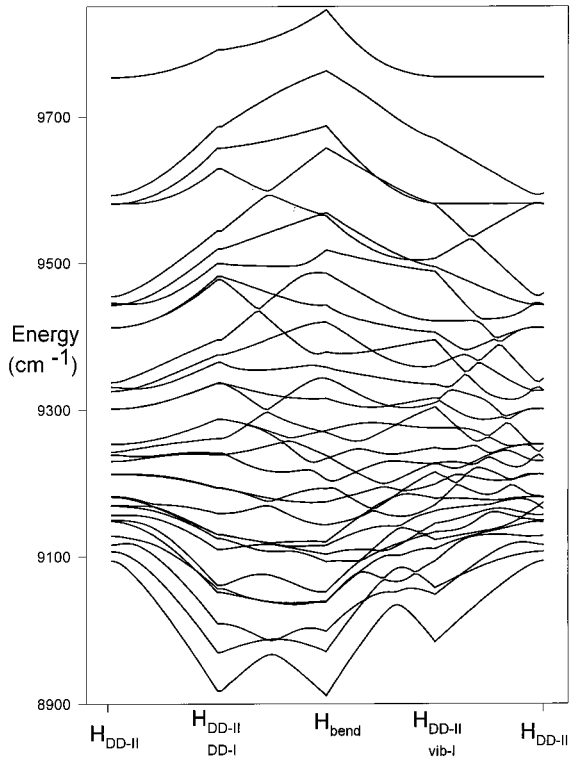

Figure 6. Adiabatic correlation diagram for polyad 14 showing levels of various partial Hamiltonians, with levels of full bend Hamiltonian in center.

bends. Finally, to get $\hat{\mathbf{H}}_{\text{bend}}$, we switch on $\hat{\mathbf{V}}_{\text{vib}-l}$ and obtain the levels at the center of the diagram. A second sequence is shown from the right, again starting with $\hat{\mathbf{H}}_0 + \hat{\mathbf{V}}_{\text{DD}-\text{II}}$. The couplings $\hat{\mathbf{V}}_{\text{vib}-l}$ and $\hat{\mathbf{V}}_{\text{DD}-\text{I}}$ are then switched on in order, again ending in the center with $\hat{\mathbf{H}}_{\text{bend}}$. It is evident that it is $\hat{\mathbf{V}}_{\text{vib}-l}$ that actually has the most pronounced effect on the energy levels of the polyad, even though the Darling−Dennison coupling $\hat{\mathbf{V}}_{\text{DD}-\text{I}}$ is primary in the sense that it is source of the initial transfer of energy from the zero-order bright state (10, 0; 0, 0).

Figures 5 and 6 show the analogous adiabatic curves for $P = 12$ and 14.

Figure 7 shows the *diabatic* curves for $P = 10$. These are nearly identical in appearance to the adiabatic curves of Figure 4; the curves are easy to follow across the avoided crossings. The diabatic curves for $P = 12$, omitted for brevity, are less straightforward because the avoided crossings are becoming larger. $P = 14$, whose diabatic curves are again omitted for brevity, is more difficult still, but it was possible to pick out diabatic curves; we will return to $P = 14$ shortly.

When difficulties arise because of large or multiple avoided crossings, following the "two-sided" adiabatic correlation diagrams of Figures 4−6 helps resolve the ambiguities. However, experimentation shows that there can be easier ways to follow the diabatic curves than turning on the couplings sequentially. A way we have found that seems to work well is to switch on all the couplings together, a proposal also successfully used by Jacobson et al.[33] This method is shown in Figures 8 and 9 for polyads $P = 12$, 14. Following the diabatic curves is "cleaner" than in Figures 5 and 6, because putting in all the couplings together tends to minimize troubles with large avoided crossings caused by any single coupling.

At each step in the diabatic correlation diagrams we possess an "assignment" of every level in terms of a set of nominal or effective quantum numbers $(n_4, l_4; n_5, l_5)^{\text{nom}}$ obtained by

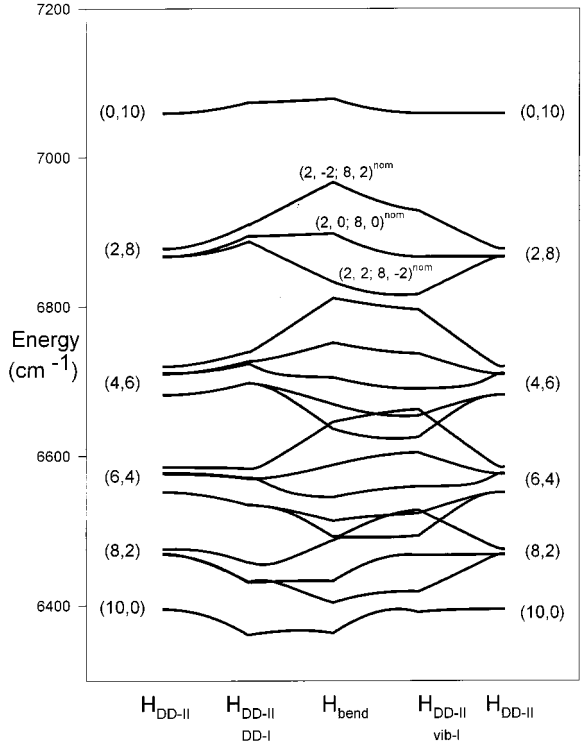

Figure 7. Diabatic correlation diagram for polyad 10 showing levels of various partial Hamiltonians, with levels of full bend Hamiltonian in center. Nominal assignments from diabatic correlation, described in section VI, are shown for three of the levels.

continuing the labels $(n_4, l_4; n_5, l_5)$ of a zero-order level along its diabatic curve, the procedure used previously for H_2O in ref 13. The multiplicity of ways of forming the correlation diagrams enables consistency checks of the nominal assignments that are made, when large or multiple avoided crossings make an

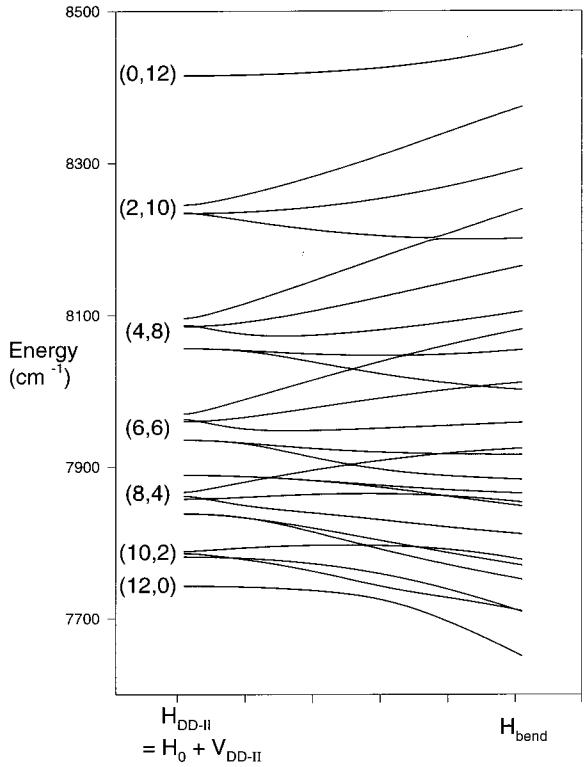

Figure 8. Diabatic correlation diagram for polyad 12, starting with $\hat{\mathbf{H}}_0 + \hat{\mathbf{V}}_{DD-II}$ at left and switching on $\hat{\mathbf{V}}_{DD-I}$ and $\hat{\mathbf{V}}_{vib-l}$ together to give levels of full bend Hamiltonian $\hat{\mathbf{H}}_{bend}$ at right.

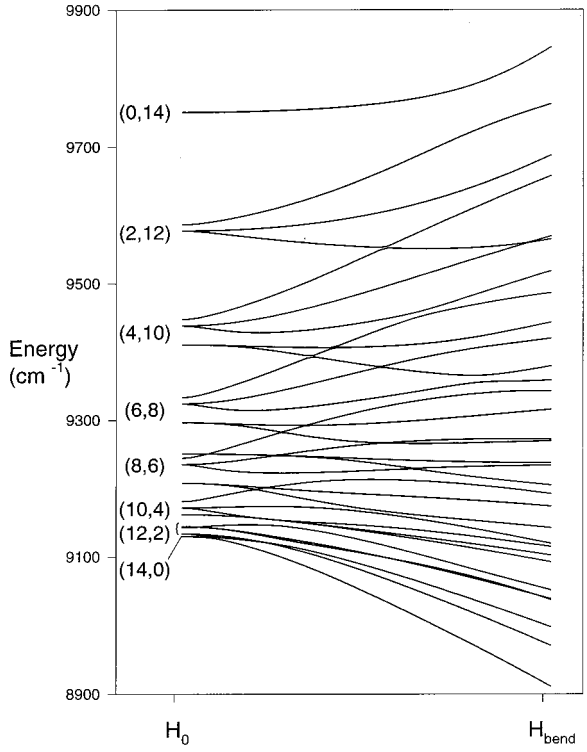

Figure 9. Diabatic correlation diagram for polyad 14, starting with $\hat{\mathbf{H}}_0 + \hat{\mathbf{V}}_{DD-II}$ at left and switching on $\hat{\mathbf{V}}_{DD-I}$ and $\hat{\mathbf{V}}_{vib-l}$ together to give levels of full bend Hamiltonian $\hat{\mathbf{H}}_{bend}$ at right.

assignment problematic in any individual correlation diagram. As examples, Figure 7 shows detailed assignments (n_4, l_4; n_5, l_5)^{nom} for the three levels of the cluster (2, 8) of polyad 10. The object of the rest of this paper is to understand the use and meaning of these assignments.

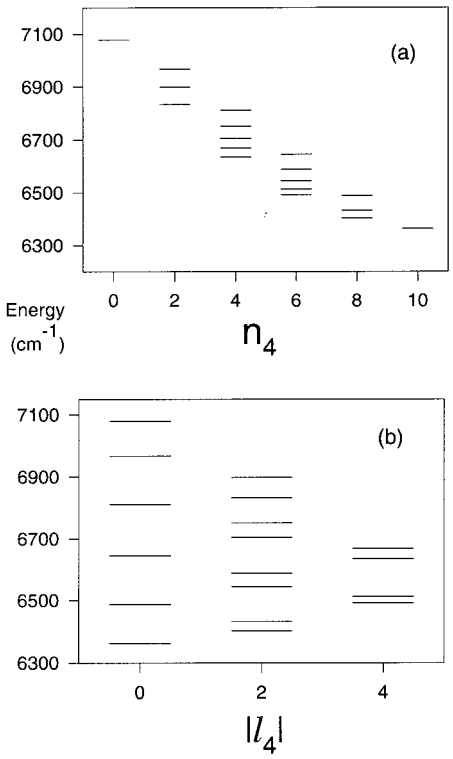

Figure 10. Polyad 10 spectrum organized into subpolyads. (a) n_4 subpolyad classification, or "subpolyads of the l-resonance"; (b) l_4 subpolyad classification, or "subpolyads of the Darling-Dennison-I resonance". The leftmost column in (b) is the primary subpolyad. See section VII for terminology.

VII. Subpolyads of the Resonances

It is evident from inspection of the diabatic correlation diagrams that the levels of $\hat{\mathbf{H}}_{bend}$ fall into fairly regular groupings or clusters, just as the intensities in Figure 2 suggested regular patterns. We want to explore the nature of both the energy and intensity patterns.

The groupings most immediately apparent in Figures 4−9 are the clusters of levels strongly split by the l-resonance at the final stage of the diabatic correlation diagram. They have common values of $(n_4, n_5)^{nom}$ but different $(l_4, l_5)^{nom}$. The clusters are therefore analogous to a sequence or subpolyad in the nominal quantum numbers $(l_4, l_5)^{nom}$. Each subpolyad can be labeled by its nominal n_4 because the total number of bend quanta $P = n_{bend} = n_4 + n_5$ is fixed. (Labeling with the nominal n_5 of course is completely equivalent.)

Polyad 10 is broken out into the n_4 subpolyads in Figure 10a. It is evident from Figures 4−6 that the splittings within the n_4 subpolyads are determined predominantly by the vibrational l-resonance coupling $\mathbf{V}_{vib-l}$, and we speak of the n_4 subpolyads also as "subpolyads of the l-resonance".

Although the l -resonance has the largest effect on the energy level pattern of the spectrum, the Darling-Dennison resonance $\hat{\mathbf{V}}_{DD-I}$ is source of the primary coupling pathway out of the zero-order bright state ($n_4 = n_{bend} = P$, $n_5 = l_4 = l_5 = 0$), as discussed earlier. As such, it is expected to be the dominant factor in the intensity pattern. An alternative grouping is then into "subpolyads of the DD−I resonance". This is a grouping into sets with common value of the nominal quantum numbers $(l_4, l_5)^{nom}$. This subpolyad organization is shown for polyad 10 in Figure 10b. The subpolayds are labeled by the nominal value of $|l_4|$; we could equally well use the nominal $|l_5|$.

Viewed through the lens of either the n_4 or the l_4 subpolyad classification, there are evident regularities in the spectral

patterns of Figure 10. How can we account for these? We will think about the problem in terms of dressed basis ideas, which we will then apply in a simplified way to interpret the patterns in detail.

In the context of the dressed basis, we can think about the n_4 subpolyad groupings in a picture in which each n_4 subpolyad originates in a sequence of zero-order states dressed by the resonances $\hat{\mathbf{V}}_{\mathrm{DD-I}}$ and $\hat{\mathbf{V}}_{\mathrm{DD-II}}$. These dressed zero-order states are then coupled to each other by a residual effective resonance $\hat{\mathbf{V}}^{\mathrm{eff}}_{\mathrm{vib}-l}$. This gives approximate subpolyads that one hopes would be close to the n_4 "subpolyads of the l resonance" of the full bend Hamiltonian $\hat{\mathbf{H}}_{\mathrm{bend}}$, the organization of the spectrum introduced in Figure 10a.

Following this line of reasoning, does it make sense to think of the l_4 "subpolyads of the DD-I resonance" of Figure 10b in terms of an alternate dressed basis? This would have zero-order states dressed by the resonances $\hat{\mathbf{V}}_{\mathrm{vib}-l}$ and $\hat{\mathbf{V}}_{\mathrm{DD-II}}$, with the dressed zero-order states coupled by an effective residual Darling-Dennison resonance $\hat{\mathbf{V}}^{\mathrm{eff}}_{\mathrm{DD-I}}$.

Perhaps, then, in forming the dressed basis one can "slice" the polyad into subpolyads whichever way one likes. This is what we have found[14] in numerical tests of the dressed basis idea on H_2O. Then the choice of the subpolyad slicing with its $\hat{\mathbf{V}}^{\mathrm{eff}}_{\mathrm{i}}$ is made for convenience, that is to say, according to the particular questions about the spectrum one is trying to answer.

For analyzing the C_2H_2 spectrum of Figure 2 and ref 3, the l_4 subpolyads with residual $\hat{\mathbf{V}}^{\mathrm{eff}}_{\mathrm{DD-I}}$ are probably most useful, because the coupling $\hat{\mathbf{V}}_{\mathrm{DD-I}}$ of $\hat{\mathbf{H}}_{\mathrm{bend}}$ dominates the intensities, being the primary pathway of energy transfer from the initially excited bright state. We proceed to use the l_4 subpolyads and the notion of an effective coupling $\hat{\mathbf{V}}^{\mathrm{eff}}_{\mathrm{DD-I}}$, to identify and account for regularities in both the energies and intensities, and analyze their dynamical meaning.

VIII. Patterns in the Subpolyads

We focus on the primary l_4 subpolydads of eigenlevels, that is, the subset of eigenlevels from each polyad with nominal quantum number $l_4^{\mathrm{nom}} = 0$, in analogy to the primary subpolyad slice of the zero-order spectrum. For polyad 10 this is the column of levels labeled $|l_4| = 0$ at the left in Figure 10b. We focus on the primary subpolyad because it dominates the intensities in each polyad; the example that will be examined in detail is the spectrum seen in Figure 2 for polyad 14. We will look at how the energy and intensity patterns can be understood in terms of the notion of an effective Darling-Dennison coupling $\hat{\mathbf{V}}^{\mathrm{eff}}_{\mathrm{DD-I}}$, acting on a basis of zero-order states dressed by the other couplings $\hat{\mathbf{V}}_{\mathrm{vib}-l}$ and $\hat{\mathbf{V}}_{\mathrm{DD-II}}$.

First, the energy level patterns. In Figures 11−13, the primary subpolyad for polyads 10, 12, and 14 is shown as successive terms in the Hamiltonian are turned on: at the left, $\hat{\mathbf{H}}_0$; then $\hat{\mathbf{V}}_{\mathrm{DD-I}}$; then $\hat{\mathbf{V}}_{\mathrm{DD-II}}$; and at the right the full bending Hamiltonian $\hat{\mathbf{H}}_{\mathrm{bend}}$ obtained with addition of $\hat{\mathbf{V}}_{\mathrm{vib}-l}$. It is evident that the couplings $\hat{\mathbf{V}}_{\mathrm{DD-I}}$ and $\hat{\mathbf{V}}_{\mathrm{vib}-l}$ exert a strong influence, with the influence of $\hat{\mathbf{V}}_{\mathrm{DD-II}}$ very small.

In Polyad 10, Figure 11, $\hat{\mathbf{H}}_0$ by itself has a pattern of monotonically increasing spacing of adjacent levels. The pattern of spacings of adjacent levels has been identified as a key to decoding internal molecular dynamics from spectra;[16] the monotonic pattern of Figure 11 is indicative of an undivided classical phase space. Adding the coupling $\hat{\mathbf{V}}_{\mathrm{DD-I}}$ in Figure 11b changes the pattern slightly, as does adding the small coupling $\hat{\mathbf{V}}_{\mathrm{DD-II}}$ in Figure 11c. However, adding $\hat{\mathbf{V}}_{\mathrm{vib}-l}$ in Figure 11d has a telling effect: the top pair in the subpolyad are pushed together, suggesting that a separatrix has been formed in the phase space of $\mathbf{H}_{\mathrm{bend}}$.

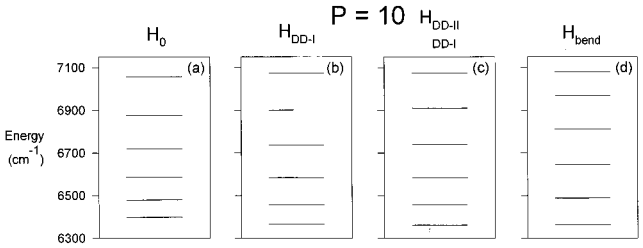

Figure 11. Spectrum of primary subpolyad of polyad 10 for various Hamiltonians including $\hat{\mathbf{H}}_0$ at left and full bend Hamiltonian $\hat{\mathbf{H}}_{\mathrm{bend}}$ at right, with partial Hamiltonians in middle columns.

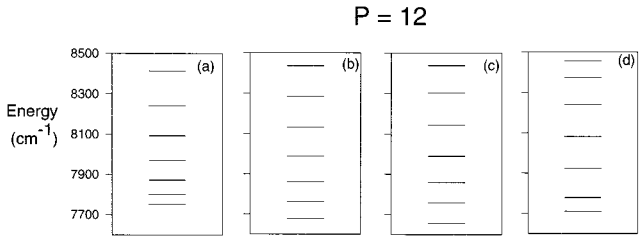

Figure 12. Spectrum of primary subpolyad of polyad 12 for various Hamiltonians including $\hat{\mathbf{H}}_0$ at left and full bend Hamiltonian $\hat{\mathbf{H}}_{\mathrm{bend}}$ at right, with partial Hamiltonians in middle columns.

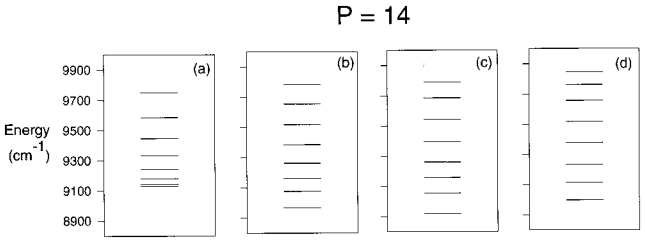

Figure 13. Spectrum of primary subpolyad of polyad 14 for various Hamiltonians including $\hat{\mathbf{H}}_0$ at left and full bend Hamiltonian $\hat{\mathbf{H}}_{\mathrm{bend}}$ at right, with partial Hamiltonians in middle columns.

In polyad 12, the effect of $\hat{\mathbf{V}}_{\mathrm{vib}-l}$ is even more apparent in Figure 12d, with a clear minimum in the level spacing for both the top and bottom pairs. In polyad 14, in Figure 13b, $\hat{\mathbf{V}}_{\mathrm{DD-I}}$ causes a minimum in spacing between levels 2 and 3. But in Figure 13d, with the full bend Hamiltonian, $\hat{\mathbf{V}}_{\mathrm{vib}-l}$ has made this disappear; nor is a minimum at the bottom pair strongly evident, unlike polyads 10 and 12. However, $\hat{\mathbf{V}}_{\mathrm{vib}-l}$ again causes a minimum at the top pair.

Clearly, the presence of the various resonance couplings, alone and in combination, causes subtle but perhaps significant changes in the energy level patterns, of a kind that indicates important phase space structure when observed in single-resonance systems.

Now, the intensity patterns. These are calculated from the eigenvectors of the spectroscopic Hamiltonian. The intensities within each polyad are assumed to originate from a single, distinct zero-order bright state, with the intensity of each level determined by the contribution of the polyad bright state to the given eigenvector. As noted above in section II, it is an assumption that each polyad originates from a *single* zero-order bright state; however, this simplification has proven empirically[3−5] to be valid for the C_2H_2 bends spectra considered here.

The intensities are shown in Figures 14−16. The top panel of each figure shows the intensities of the primary subpolyad calculated with just the terms $\hat{\mathbf{H}}_0 + \hat{\mathbf{V}}_{\mathrm{DD-I}}$. The middle panel

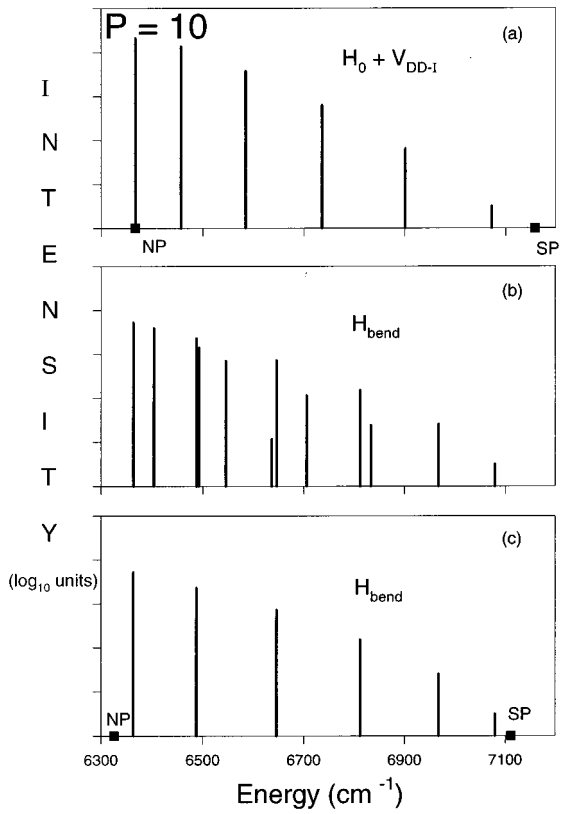

Figure 14. Intensities (log_{10} scale, arbitrary units) of polyad 10 states (a) for levels of primary subpolyad, calculated with partial Hamiltonian $\hat{\mathbf{H}}_0 + \hat{\mathbf{V}}_{DD-I}$; (b) for all levels, calculated with full bend Hamiltonian $\hat{\mathbf{H}}_{bend}$; (c) for levels of primary subpolyad, calculated with full bend Hamiltonian $\hat{\mathbf{H}}_{bend}$. Fixed points notation: north pole NP; south pole SP (see also Figure 17).

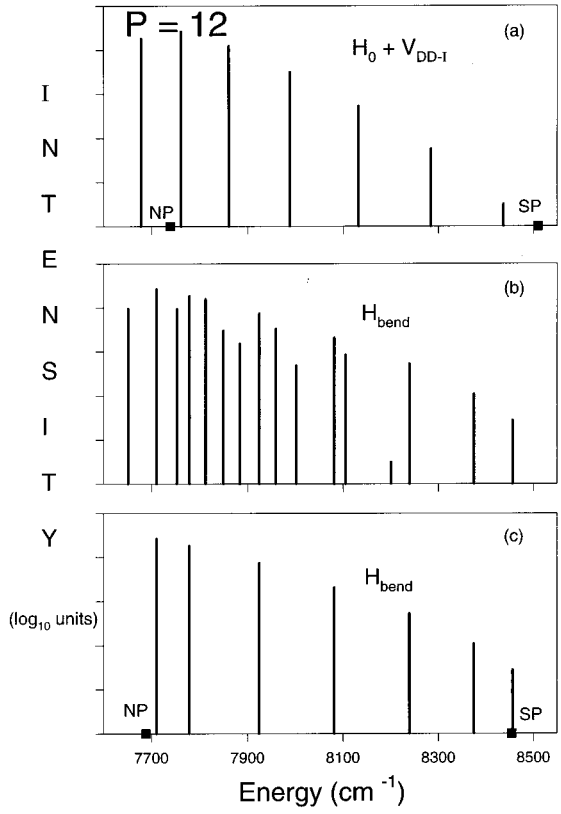

Figure 15. Intensities (log_{10} scale, arbitrary units) of polyad 12 states (a) for levels of primary subpolyad, calculated with partial Hamiltonian $\hat{\mathbf{H}}_0 + \hat{\mathbf{V}}_{DD-I}$; (b) for all levels, calculated with full bend Hamiltonian $\hat{\mathbf{H}}_{bend}$; (c) for levels of primary subpolyad, calculated with full bend Hamiltonian $\hat{\mathbf{H}}_{bend}$. Fixed points notation: north pole NP; south pole SP (see also Figure 17).

shows the intensities of the entire polyad calculated with the full bending Hamiltonian $\hat{\mathbf{H}}_{bend}$. The bottom panel again shows the intensities of the primary subpolyad alone, but calculated with the full bend Hamiltonian $\hat{\mathbf{H}}_{bend}$.

For polyad 10, the intensities with just $\hat{\mathbf{V}}_{DD-I}$ in Figure 14a monotonically decrease. The pattern is little changed in part c with $\hat{\mathbf{V}}_{vib-l}$. For polyad 12, with $\hat{\mathbf{V}}_{DD-I}$ alone in Figure 15a, the second level is most intense, but with $\hat{\mathbf{V}}_{vib-l}$ added in part c, the first level is most intense. For polyad 14 in Figure 16a, $\hat{\mathbf{V}}_{DD-I}$ alone makes the third level most intense, but with $\hat{\mathbf{V}}_{vib-l}$ in part c, the second level is significantly more intense.

Is there really dynamical meaning nested in these energy and intensity patterns? If so, we would like to give an account in terms of the notion of an effective $\hat{\mathbf{V}}^{eff}_{DD-I}$ acting on "zero-order" states which enfold $\hat{\mathbf{V}}_{vib-l}$ and $\hat{\mathbf{V}}_{DD-II}$.

IX. Single-Resonance Fit of the Primary Subpolyads

One way to test this would be to fit the entire spectrum with a dressed basis Hamiltonian with an effective Darling−Dennison−I coupling

$$\hat{\mathbf{H}}^{dr}_{bend} = \hat{\mathbf{H}}^{dr}_0 + \hat{\mathbf{V}}^{eff}_{DD-I} \tag{7}$$

with

$$\hat{\mathbf{H}}^{dr}_0 = \hat{\mathbf{H}}_0 + \hat{\mathbf{V}}_{vib-l} + \hat{\mathbf{V}}_{DD-II} \tag{8}$$

Here we have attempted something simpler, which nonetheless shares some aspects of the dressed basis idea. Rather than a global fit with a dressed basis, we fit a subset of the levels with a very simple, six-parameter single-resonance Hamiltonian:

$$\hat{\mathbf{H}}^{fit} = \hat{\mathbf{H}}^{fit}_0 + \hat{\mathbf{V}}^{fit}_{DD-1} = \omega^0_4 n_4 + \omega^0_5 n_5 + \chi_{44} n_4^2 + \chi_{45} n_4 n_5 + \chi_{55} n_5{}^2 + K[a^\dagger_{4+} a^\dagger_{4-} a_{5+} a_{5-} + \text{h.c.}] \tag{9}$$

Note the use in (9) of a zero-order energy formula given in the standard way by terms linear and quadratic in the zero-order quantum numbers, which here are to be understood in the sense of nominal quantum numbers for a dressed basis which is not explicitly defined or calculated. In a true dressed basis approach, the dressed zero-order Hamiltonian $\hat{\mathbf{H}}^{dr}_0$ would not be given by a polynomial in the quantum numbers. The price we pay for using the simplified zero-order energy formula (9) instead of a true dressed basis is that we can only fit a subset of levels of the entire spectrum—otherwise a multiresonance fitting Hamiltonian like $\hat{\mathbf{H}}_{bend}$ would not have been necessary in the first place. Still, this fit should have something of the dressed basis idea built into it, because the zero-order energies obtained in the fit to (9) definitely must be strongly influenced by and reflect the resonance couplings $\hat{\mathbf{V}}_{vib-l}$ and $\hat{\mathbf{V}}_{DD-II}$. The Darling−Dennison coupling $\hat{\mathbf{V}}^{fit}_{DD-1}$ in (9) therefore plays a role like a residual effective coupling $\hat{\mathbf{V}}^{eff}_{DD-1}$ in a true dressed basis fit.

We included in the data set the 21 levels of the primary subpolyads of polyads 10, 12, and 14. We fit only the energies, leaving the intensities as predictions of the fit. If the fit can reproduce both the energy level and intensity patterns of the subpolyads, a further test will be whether the semiclassical dynamics inferred from the fit give a coherent explanation of the observed spectral patterns.

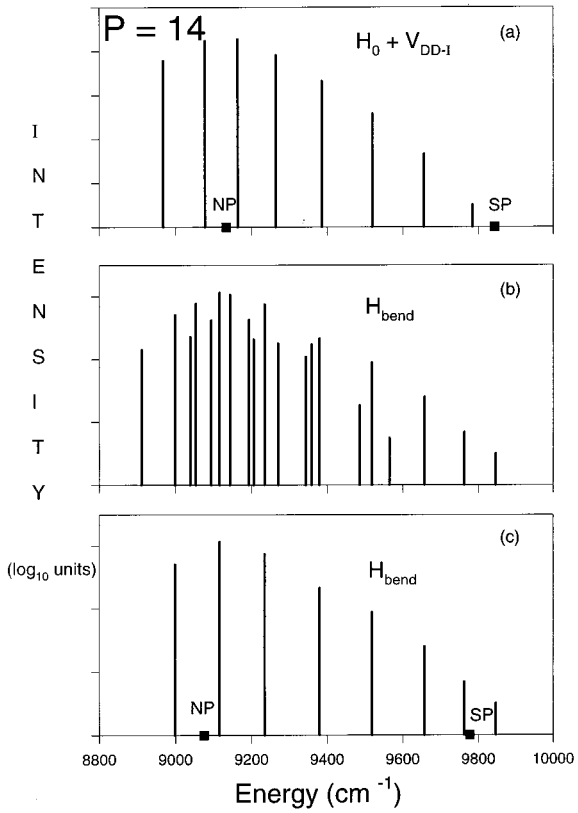

Figure 16. Intensities (log_{10} scale, arbitrary units) of polyad 14 states (a) for levels of primary subpolyad, calculated with partial Hamiltonian $\hat{\mathbf{H}}_0 + \hat{\mathbf{V}}_{DD-I}$; (b) for all levels, calculated with full bend Hamiltonian $\hat{\mathbf{H}}_{bend}$; (c) for levels of primary subpolyad, calculated with full bend Hamiltonian $\hat{\mathbf{H}}_{bend}$. Fixed points notation: north pole NP; south pole SP (see also Figure 17).

The results of the fit are shown in Tables 3 and 4. The values of the fitted parameters for $\hat{\mathbf{H}}^{fit}$ seemingly differ little from their corresponding values in $\hat{\mathbf{H}}_{bend}$. Does this $\hat{\mathbf{H}}^{fit}$ account for the observed patterns in the energy levels and intensities? And do the differences between corresponding parameters in $\hat{\mathbf{H}}^{fit}$ and $\hat{\mathbf{H}}_{bend}$ have intelligible dynamical significance?

X. Phase Spheres

To answer this, we used the fit to construct polyad phase spheres, a way of representing and visualizing the spectrum in phase space. The phase sphere was first developed for a system of two modes coupled by a single resonance;[21] didactic presentations can be found in refs 17 and 18. The phase sphere projects out the conserved polyad number and its conjugate angle, leaving a semiclassical representation of each energy level of a polyad on a reduced phase space, which is properly represented on a sphere.[34,35]

The spheres for polyads 10, 12, and 14 are shown in Figure 17. The spheres show considerable phase space structure, with separatrices dividing regions of vibrational motion of different character. The three kinds of motion observed are local and normal bend modes, and the "precessional modes" identified[15] in a single-resonance model of the acetylene bends as an instance of a novel kind of vibrational motion[36] for the Darling−Dennison Hamiltonian.

How well do the phase spheres account for the observed energy and intensity patterns? The sphere for polyad 10 has a separatrix at the north pole, dividing a tiny local mode region from a normal mode region that covers most of the sphere. Near the south pole, another separatrix divides the normal region from a tiny precessional modes region. All the quantum states correspond to trajectories of normal mode character, but the separatrices are expected to influence the spectral pattern. A classical separatrix is predicted[16] to induce a minimum in the level spacing, and this minimum has been observed in several systems.[37,38] In polyad 10, the separatrices near the north and south poles are at the low and high energy ends of the subpolyad.

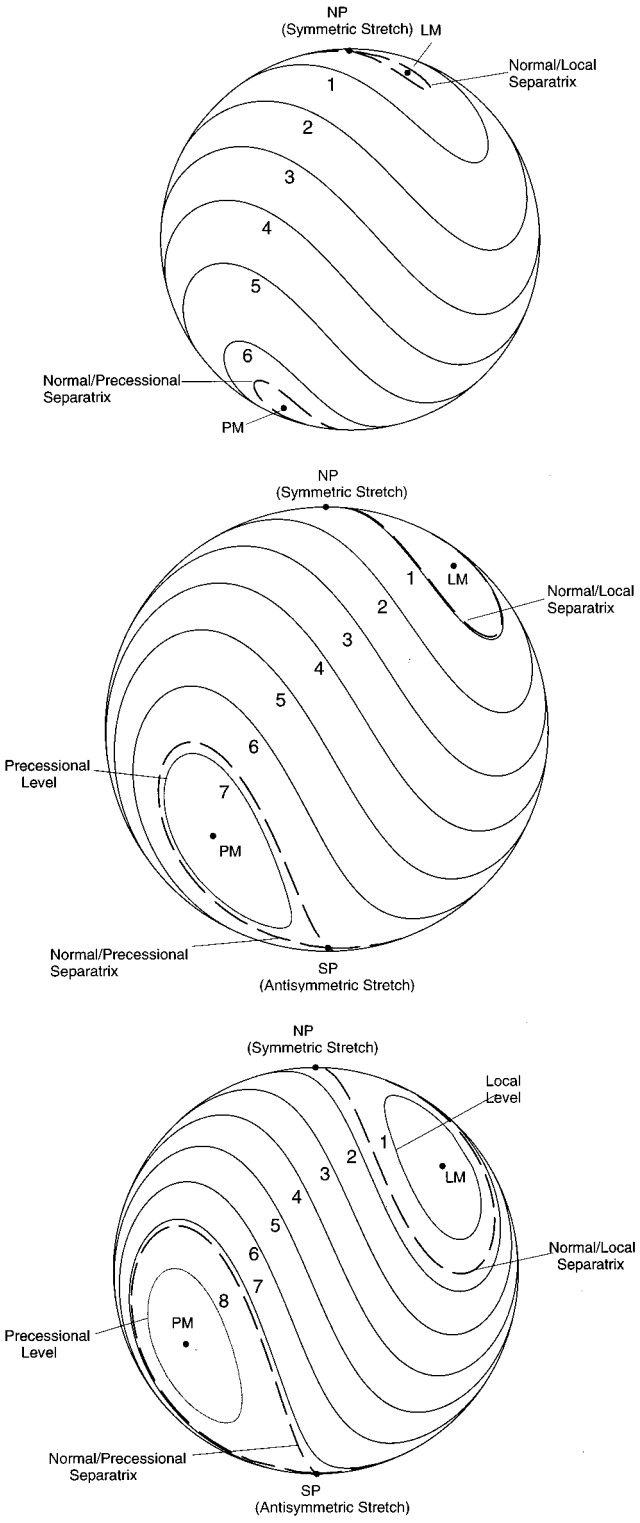

Figure 17. Polyad phase spheres from fit of primary subpolyads of polyad 10, 12, 14 to a single-resonance Hamiltonian, described in section IX. Each sphere shows the primary subpolyad from one polyad 10, 12, or 14. Fixed points notation: north pole NP; south pole SP; local mode LM; precessional mode PM.

TABLE 3: Fit Summary for Parameters

parameters (cm^{-1})	$\hat{\mathbf{H}}_{bend}$	$\hat{\mathbf{H}}^{fit}$
	605.258[a]	601.830
ω_5^0	736.246[b]	731.897
χ_{44}	3.082	3.050
χ_{45}	−2.406	1.012
χ_{55}	−2.335	−2.3348
K	−10.0	−12.498

[a] In terms of the parameters from Table 2, $\omega_4^0 = \omega_4 + (\chi_{14} + \chi_{24} + \chi_{34})/2$. [b] In terms of the parameters from Table 2, $\omega_5^0 = \omega_5 + (\chi_{15} + \chi_{25} + \chi_{35})/2$.

TABLE 4. Fit summary of Energy Levels: RMS = 9.25

	energies (cm^{-1})			
polyads	assignment[a]	calculated[b]	fitted	residual
10	(10,0;0,0)	6363.62	6364.15	−0.53
10	(8,0;2,0)	6487.74	6491.56	−3.82
10	(6,0;4,0)	6646.10	6647.06	−0.96
10	(4,0;6,0)	6811.98	6809.00	2.98
10	(2,0;8,0)	6967.38	6961.30	6.08
10	(0,0;10,0)	7079.10	7081.66	−2.56
12	(12,0;0,0)	7710.33	7690.53	19.80
12	(10,0;2,0)	7778.27	7793.90	−15.63
12	(8,0;4,0)	7924.04	7931.62	−7.58
12	(6,0;6,0)	8081.45	8083.30	−1.85
12	(4,0;8,0)	8239.33	8233.59	5.74
12	(2,0;10,0)	8374.31	8366.69	7.62
12	(0,0;12,0)	8455.53	8465.59	−10.06
14	(14,0;0,0)	8998.49	9016.01	−17.52
14	(12,0;2,0)	9115.40	9112.94	2.45
14	(10,0;4,0)	9234.49	9229.95	4.54
14	(8,0;6,0)	9379.74	9368.75	10.99
14	(6,0;8,0)	9518.59	9513.04	5.55
14	(4,0;10,0)	9657.77	9648.844	8.92
14	(2,0;12,0)	9762.47	9760.42	2.05
14	(0,0;14,0)	9845.63	9861.78	−16.15

[a] Nominal assignment from correlation diagrams. The quantum number scheme is described in section VI. [b] From spectroscopic Hamiltonian $\hat{\mathbf{H}}_{bend}$.

This is consistent with the minima in the level spacings noted in Figure 11d. In particular, this accounts for the formation of the minimum in the spacing at the high energy pair in going from Figure 11a−c to Figure 11d, so the spectral fit with $\hat{\mathbf{V}}_{DD-1}^{fit}$ accounts nicely for the energy pattern of the subpolyad.

Now we consider the intensities. In the phase sphere for the zero-order system, a circumpolar trajectory near the north pole corresponds to the quantum zero-order bright state. In the phase sphere with $\hat{\mathbf{V}}_{DD-1}^{fit}$ in Figure 17a, the states corresponding to trajectories nearest the north pole are expected to have the greatest intensity, with a rapid intensity falloff from the lowest energy (nearest north pole) state of the subpolyad. This is exactly what was noted in Figure 14.

The phase sphere for polyad 12 in Figure 17b again has two separatrices. Now there is a quantum level almost on the separatrix near the north pole, and a precessional level inside the separatrix near the south pole. The prediction is that the level spacing minima at the top and bottom of the subpolyad should be quite distinct, exactly what was noted for polyad 12 in Figure 12d. The prediction for the intensities is that state 1 should be most intense, since it is very near the north pole, with monotonically decreasing intensity for the other states. This is exactly what was observed in Figure 15c. Note that the Hamiltonian $\hat{\mathbf{H}}_0 + \hat{\mathbf{V}}_{DD-I}$ in Figure 15a did not get this right: it has state 2 highest in intensity. This shows that the small differences in Table 3 for the parameters of the two Hamiltonians do lead to subtly distinct but meaningful spectral patterns, with the Hamiltonian $\hat{\mathbf{H}}^{fit}$ giving the correct pattern, which is then explained by the phase sphere inferred from $\hat{\mathbf{H}}^{fit}$.

Finally, the phase sphere for polyad 14 has two separatrices. States 1 and 2 are on opposite sides of the separatrix at the north pole, so at the low end of the subpolyad, a clear minimum is expected, just as observed in Figure 13(d). At the high energy end, state 7 is barely outside the separatrix, with state 8 well on the other side of the separatrix. This predicts a minimum between states 7 and 8, but one which is not too pronounced, and this is what was noted in Figure 13d. For the intensities, state 2 is nearest the north pole, so should be most intense, exactly as observed in Figure 16(c). Note that the naive Hamiltonian $\hat{\mathbf{H}}_0 + \hat{\mathbf{V}}_{DD-I}$ predicts that state 3 should be most intense, as in Figure 16a, showing again how distinct spectral markers arise from subtle parameter differences in the Hamiltonian $\hat{\mathbf{H}}^{fit}$.

XI. Conclusions

We have shown that we can identify energy and intensity patterns in the pure bends spectrum of acetylene with diabatic correlation diagrams and the nominal effective quantum number assignment procedure, classifying the spectrum into subpolyad sequences. Fits of the spectra to a resonance Hamiltonian with some of the features of the dressed basis approach[14] yield polyad phase spheres. The phase spheres give a successful account of all the regularities observed in the energy and intensity patterns, in terms of phase space structure and bifurcations of the normal modes.

This shows that there is great scope for detailed analysis of high energy spectra involving many degrees of freedom, multiple resonances, and chaotic classical dynamics. The treatment here with nominal assignments of subpolyad sequences and phase spheres gives a novel view of energy and intensity patterns within polyads of the acetylene bends spectrum. However, this is certainly not yet near a complete treatment of the spectrum, since only the primary subpolyads of polyads 10, 12, and 14 have been included. It was noted in section II that in Figure 2 there appear to be sequences visible to "eyeball" inspection, as also in the logarithmic plot of the same spectrum in Figure 16b. The primary subpolyad shown in Figure 16(c) in fact has been revealed here as a kind of sequence. However, there are further evident regularities in Figures 14b−16b awaiting scrutiny. In the progression from polyad 10 to polyad 14, the degree of classical chaos is increasing greatly, but in polyad 14 in Figure 16b, there is still evident regularity in the overall envelope of the intensity pattern, and regularities in the detailed structure of intensities within the envelope. Furthermore, the question of regularity in the most chaotic portion of the pure bends spectrum lies ahead at polyads 16−18. (At higher polyads, the spectrum actually becomes more regular again.[7])

Others have made considerable progress on semiclassical analysis of the acetylene bends spectrum, in particular, using bifurcation analysis. Jacobson and co-workers have shown[33] that the local modes representation is superior for higher polyad numbers; with Taylor and Jung, they have given a bifurcation analysis[39] of the $P = 22$ polyad. Prosmiti and Farantos[40] have considered numerically on a potential surface a number of the periodic orbits born in bifurcations; McCoy and Sibert[41] have considered periodic orbits of a potential surface obtained from the experimental spectrum.

A complete treatment of the spectrum along the lines developed here is now a plausible goal. This will involve a full-blown application of the dressed basis approach, combined with

a complete bifurcation analysis of the spectroscopic Hamiltonian of the kind already performed for triatomics.[13,42] We are currently pursuing this.

Future challenges for the diabatic assignment technique include using spectra to elucidate the pathway to the acetylene-vinylidene isomerization, and treatment of spectra with stretch as well as bend vibrations. We have already obtained results comparable to those here for a planar model of acetylene which includes the stretch modes.[43] The power of bifurcation analysis of spectra for ultrafast intramolecular rearrangement processes has been demonstrated for the isomerization spectrum of HCP.[37]

References and Notes

(1) Jonas, D. M.; Solina, S. A. B.; Rajaram, B.; Silbey, R. J.; Field, R. W.; Yamanouchi, K.; Tsuchiya, S. *J. Chem. Phys.* **1993**, *99*, 7350.
(2) Jonas, D. M. Ph.D. Dissertation, Massachusetts Institute of Technology, 1992.
(3) Solina, S. A. B.; O'Brien, J. P.; Field, R. W.; Polik, W. F. *Ber. Bunsen-Ges. Phys. Chem.* **1995**, *99*, 555.
(4) Solina, S. A. B.; O'Brien, J. P.; Field, R. W.; Polik, W. F. *J. Phys. Chem.* **1996**, *100*, 7797.
(5) O'Brien, J. P.; Jacobson, M. P.; Sokol, J. J.; Coy, S. L.; Field, R. W. *J. Chem. Phys.* **1998**, *108*, 7100.
(6) Jacobson, M. P.; O'Brien, J. P.; Silbey, R. J.; Field, R. W. *J. Chem. Phys.* **1998**, *109*, 121.
(7) Jacobson, M. P.; O'Brien, J. P.; Field, R. W. *J. Chem. Phys.* **1998**, *109*, 3831.
(8) Abbouti Temsamani, M.; Herman, M *J. Chem. Phys.* **1995**, *102*, 6371.
(9) Abbouti Temsamani, M.; Herman, M.; Solina, S. A. B.; O'Brien, J. P.; Field, R. W. *J. Chem. Phys.* **1996**, *105*, 11357.
(10) El Idrissi, M. I.; Lievin, J.; Campargue, A.; Herman, M. *J. Chem. Phys.* **1999**, *110*, 2074.
(11) Kellman, M. E. *J. Chem. Phys.* **1990**, *93*, 6330.
(12) Kellman, M. E.; Chen, G. *J. Chem. Phys.* **1991**, *95*, 8671.
(13) Rose, J. P.; Kellman, M. E. *J. Chem. Phys.* **1996**, *105*, 7348.
(14) Kellman, M. E.; Dow, M. W. *J. Chem. Phys.* **2000**. Submitted for publication.
(15) Rose, J. P.; Kellman, M. E. *J. Chem. Phys.* **1996**, *105*, 10743.
(16) Svitak, J.; Li, Z.; Rose, J. P.; Kellman, M. E. *J. Chem. Phys.* **1995**, *102*, 4340.
(17) Kellman, M. E. *Annu. Rev. Phys. Chem.* **1995**, *46*, 395.
(18) Kellman, M. E. Dynamical Analysis of Highly Excited Vibrational Spectra: Progress and Prospects. In *Molecular Dynamics and Spectroscopy by Stimulated Emission Pumping*: *Algebraic Methods in Spectroscopy*; Dai, H.-L., Field, R. W., Eds.; World Scientific: Singapore, 1995.
(19) Kellman, M. E. *J. Chem. Phys.* **1985**, *83*, 3843.
(20) Kellman, M. E.; Lynch, E. D. *J. Chem. Phys.* **1986**, *85*, 5855.
(21) Xiao, L.; Kellman, M. E. *J. Chem. Phys.* **1989**, *90*, 6086.
(22) Kellman, M. E.; Xiao, L. *Chem. Phys. Lett.* **1989**, *162*, 486.
(23) Li, Z.; Xiao, L.; Kellman, M. E. *J. Chem. Phys.* **1990**, *92*, 2251.
(24) Xiao, L.; Kellman, M. E. *J. Chem. Phys.* **1990**, *93*, 5805.
(25) Kellman, M. E.; Xiao, L. *J. Chem. Phys.* **1990**, *93*, 5821.
(26) Rose, J. P.; Kellman, M. E. *J. Chem. Phys.* **1995**, *103*, 7255.
(27) Lu, Z.-M.; Kellman, M. E. *J. Chem. Phys.* **1997**, *107*, 1.
(28) Pliva, J. *J. Mol. Spectrosc.* **1972**, *44*, 165.
(29) Smith, B. C.; Winn, J. S. *J. Chem. Phys.* **1988**, *89*, 4638.
(30) Smith, B. C.; Winn, J. S. *J. Chem. Phys.* **1991**, *94*, 4120.
(31) Fried, L. E.; Ezra, G. S. *J. Chem. Phys.* **1987**, *86*, 6270.
(32) Kellman, M. E. *Adv. Chem. Phys.* **1997**, *101*, 590.
(33) Jacobson, M. P.; Silbey, R. J.; Field, R. W. *J. Chem. Phys.* **1999**, *110*, 845.
(34) Jaffe, C. *J. Chem. Phys.* **1988**, *89*, 3395.
(35) Kellman, M. E.; Lynch, E. D. *J. Chem. Phys.* **1988**, *89*, 3396.
(36) Gray, S. K.; Child, M. S. *Mol. Phys.* **1984**, *53*, 961.
(37) Joyeux, M.; Sugny, D.; Tyng, V.; Kellman, M. E.; Ishikawa, H.; Field, R. W. *J. Chem. Phys.* **1999**, *112*, 4162.
(38) Ishikawa, H.; Nagao, C.; Mikami, N.; Field, R. W. *J. Chem. Phys.* **1998**, *109*, 492.
(39) Jacobson, M. P.; Jung, C.; Taylor, H. S.; Field, R. W. *J. Chem. Phys.* **1999**, *111*, 66.
(40) Prosmiti, R.; Farantos, S. C. *J. Chem. Phys.* **1995**, *103*, 3299.
(41) Sibert, E. L.; McCoy, A. B. *J. Chem. Phys.* **1996**, *105*, 469.
(42) Keshavamurthy, S.; Ezra, G. S. *J. Chem. Phys.* **107**, *156*, 1997.
(43) Rose, J. P.; Kellman, M. E. 2000. Unpublished work.